ACS APPLIED MATERIALS & INTERFACES

www.acsami.org

Research Article

A Chemically Polished Zinc Metal Electrode with a Ridge-like Structure for Cycle-Stable Aqueous Batteries

Jindi Wang,[‡] Zhao Cai,[‡] Run Xiao, Yangtao Ou, Renming Zhan, Zhu Yuan, and Yongming Sun*

Cite This: *ACS Appl. Mater. Interfaces* 2020, 12, 23028–23034

Read Online

ACCESS | Metrics & More | Article Recommendations | Supporting Information

ABSTRACT: Aqueous rechargeable zinc (Zn) metal batteries show great application prospects in grid-scale energy storage devices due to their good safety, low cost, and considerable energy density. However, the electrical and topographical inhomogeneity caused by the native passivation layer of metallic Zn foil leads to inhomogeneous electrochemical plating and stripping of metallic Zn, and the limited accessible area to the electrolyte of the regular foil electrode causes the poor rate capability, which together hinder the practical application of the Zn metal electrode in rechargeable aqueous batteries. In this work, we show that the native passivation layer on the Zn foil electrode can be removed by a simple chemical polishing strategy, associated with the formation of a three-dimensional ridge-like structure of metallic Zn (r-Zn) on the surface of the Zn foil electrode due to the selective etching of weak crystallographic planes and grain boundary of metallic Zn. The clean and uniform surface of the metallic Zn electrode enables homogeneous plating and stripping of metallic Zn, and the ridge-like structure of r-Zn increases the accessible surface area to the electrolyte and reduces the local current density, which elevates the electrochemical performance of the Zn metal anode with regard to the cycling stability and rate capability. It is demonstrated that a r-Zn anode cycles stably for over 200 h at 1 mA cm^{-2} and 0.5 mA h cm^{-2} with a low overpotential of 20 mV, which far outperforms 39 h of cycling with an overpotential of 72 mV for its pristine metallic Zn counterpart.

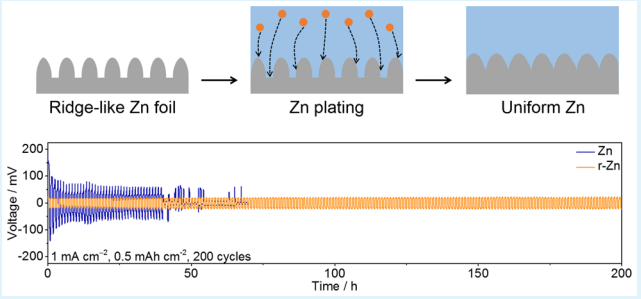

KEYWORDS: *aqueous zinc metal battery, passivation layer, chemical polishing, ridge-like structure, homogeneous plating*

1. INTRODUCTION

The use of fossil fuels produces greenhouse gases (e.g., CO_2, N_2O, and CH_4) and other environmental pollutants, which change Earth's climate system. It is of vital importance to develop technologies to utilize clean sustainable energy (e.g., wind, solar, and tide) with low cost and reduce the fossil fuel consumption in the near future.[1] However, the uneven spatial and temporal distribution of renewable energy causes a big challenge for their efficient utilization. One promising strategy to address this issue is to develop an advanced battery system with long cycle life and low cost for the storage of renewable energy before its utilization.[2,3] Among the various energy storage systems, a long-life and low-cost aqueous Zn metal battery is highly desirable.[4−9] Aqueous electrolytes are safe, green, easy to operate, and have high ionic conductivity.[10−12] Also, the Zn metal is abundant and inexpensive, and its bivalent carriers provide high capacity.[7,13] Until now, zinc-manganese dioxide (Zn-MnO_2) batteries have occupied a large part of the primary battery market. Unfortunately, the practical application of the long-life rechargeable Zn-MnO_2 battery has yet been realized despite recent great research progress. A large number of factors lead to poor cycle performance of the Zn metal battery, including dendrite growth, corrosion, and hydrogen evolution at the Zn metal anode. One of the important factors is the uncontrollable and inhomogeneous Zn deposition.[14−17] The uncontrollable deposition of Zn produces the electrical and topographical inhomogeneity of the electrode and leads to the growth of Zn dendrites, which can pierce the separator and cause short circuit of the battery. The phenomenon of dendrite growth would be more serious under large applied current densities,[18] where the large applied current density is a basic requirement for the application in smart grids for energy storage equipment.[19−21] Therefore, it is of great significance to develop long lifespan and dendrite-free Zn metal anodes for aqueous Zn metal batteries.

A complex and nonuniform native passivation layer exists on the surface of conventional Zn foil, which is composed of zinc oxide, basic zinc carbonate, and so on. Such a passivation layer leads to inhomogeneous resistance for charge transport and electric field distribution on the electrode surface during electrochemical plating and stripping of metallic Zn, thereby

Received: March 26, 2020
Accepted: April 24, 2020
Published: April 24, 2020

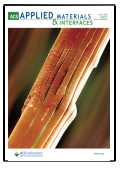

https://dx.doi.org/10.1021/acsami.0c05661
ACS Appl. Mater. Interfaces 2020, 12, 23028−23034

causes the nucleation priority of metallic Zn during its plating and dissolution priority during its stripping in some local areas, and eventually leads to the uncontrollable deposition of Zn. In the past years, great attention has been paid to homogenize the plating and stripping of metallic Zn and improve the cycle life. The nanoporous $CaCO_3$ layer was coated on the surface of the metallic Zn electrode, which homogenized the flux of Zn ions and led to uniform deposition of metallic Zn.[22] Similarly, polyamide[23] and metal−organic framework[24] surface protection layers and polymer solid electrolytes[25−29] were used to achieve uniform Zn ion flux and uniform Zn deposition. Sodium ions were introduced into the aqueous electrolyte, which could be adsorbed at the electron enrichment site of the Zn metal electrode and homogenize the electric field distribution.[30] Similarly, adding Mn^{2+} in the electrolyte could also have a positive effect on the electrochemical cycling of the Zn metal electrode.[31,32] Besides, metallic Zn electrodes with large accessible surface areas to electrolytes created by electrode structure design (e.g., porous Zn sponge[33] and interconnected 3D scaffolds[15,34−39]) greatly reduced the local current density and homogenized the surface electric field distribution and Zn ion flux, which not only improved the cycling stability but also improved the rate capability of the metallic Zn electrode. Despite the much improved electrochemical performance by the above advanced electrode structure and electrolyte engineering, these studies were mainly conducted based on the use of the pristine Zn metal. Little attention has been paid to the effect of the native surface film of the pristine Zn metal on the electrochemical performance of the Zn metal, which we think is very important for understanding the metallic Zn chemistry for aqueous batteries and realizing its practical application. Therefore, it is of great significance to investigate the electrochemical performance of the Zn metal electrode with a clean surface without the passivation layer and design advanced metallic Zn electrodes.

In this paper, we report a 3D ridge-like zinc (r-Zn) electrode fabricated via a simple ultrasonic-assisted acid etching method. The as-achieved structure shows three attractive merits for the understanding and improvement of the Zn metal electrode for rechargeable aqueous batteries: First, the impurities from the surficial passivation layer are removed during the acid etching process, which not only exposes a large amount of active Zn for facile dissolution and deposition but also homogenizes the electric field and ion flux at the electrode surface. Second, the mass transfer process is improved from planar to three-dimensional, also beneficial to improve the rate performance of the Zn metal battery. Third, the effect of the native passivation layer on the electrochemical performance of Zn metal electrodes can be systematically investigated, which can help to understand the electrochemical behavior of the Zn metal and design advanced Zn metal electrodes. As a result, the as-fabricated 3D r-Zn electrode with a fresh surface shows low overpotential (20 mV) and good cycle life (200 cycles at 0.5 mA h cm^{-2} and 1 mA cm^{-2}), which outperforms the pristine Zn metal electrode with a native passivation layer.

2. EXPERIMENTAL SECTION

2.1. Preparation of the r-Zn. The r-Zn was fabricated using commercial Zn foil (purity: 99.9 wt %, thickness: ∼200 μm) as the starting material through a chemical etching route. Typically, a pristine Zn foil was first rested in a dilute hydrochloric acid solution (6 vol %) under sonication for 5 min at ∼25 °C and then rinsed with deionized water and ethanol several times. To avoid oxidation, the Zn foil after etching and rinsing was dried by Ar blowing and stored in an Ar-filled glove box before further use and characterizations.

2.2. Characterization. The X-ray diffraction (XRD) patterns of the pristine Zn and r-Zn foils were collected on a PANalytical B.V., Holland with Cu Kα radiation (λ = 0.154 nm). The morphology and microstructure of the pristine Zn and r-Zn electrodes before and after cycling were characterized by employing a scanning electron microscope (SEM, Sirion 200).

2.3. Electrochemical Measurements. The pristine Zn and r-Zn foils were first cut into disks (Φ = 12 mm) as the electrodes for electrochemical characterizations. Zn || Zn and r-Zn || r-Zn symmetrical cells were assembled with a coin cell configuration (2032-type) in ambient conditions. Glass fiber (Φ = 16 mm) and 3 M $ZnSO_4$ were used as the separator and aqueous electrolyte, respectively. Electrochemical plating/stripping measurement of metallic Zn was performed on a Neware battery tester (Shenzhen Neware Technology Co., Ltd., China) at current densities of 1−5 mA cm^{-2} with fixed capacities of 0.2−0.5 mA h cm^{-2}. The nucleation overpotential measurement was conducted by plating metallic Zn on different electrodes (pristine Zn or r-Zn electrode) in standard CR2032 coin-type cells in the 3 M $ZnSO_4$ aqueous electrolyte. The electrochemical impedance spectrum (EIS) was collected on a Biologic VMP3 electrochemical workstation with a frequency range of 100 kHz to 0.01 Hz with an AC voltage of 5 mV.

3. RESULTS AND DISCUSSION

Figure 1 illustrates the important role of r-Zn in improving the electrochemical plating/stripping behavior of metallic Zn. A

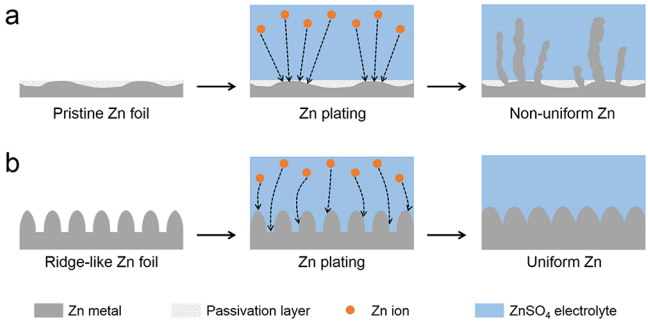

Figure 1. Schematic illustration of the Zn plating process on (a) the pristine Zn foil electrode with a native passivation layer and (b) the 3D r-Zn foil electrode with a clean surface.

native nonuniform passivation layer generally exists on pristine metallic Zn foil due to its high chemical reactivity. Such a passivation layer mainly consists of ZnO and other Zn-containing species,[40,41] which can lead to high and nonuniform surface electrochemical impedance. Further, the nonuniform local surface structure leads to nonuniform Zn plating/stripping and eventually dendrite formation (Figure 1a). In our experiment, a chemical polishing process is introduced, and the nonuniform passivation layer is removed, leaving a clean surface of metallic Zn with a uniform surface structure. The clean surface of the as-achieved Zn electrode can reduce the nucleation overpotential, and its uniform surface is beneficial for enabling uniform electrochemical plating/stripping of metallic Zn due to the more uniform electric field on the surface of the Zn metal electrode (Figure 1b). Moreover, the chemical etching produces a 3D ridge-like structure, which can increase the accessible surface area of the electrode to the electrolyte, reduce the local current density, and then the possibility for dendrite growth. Taking the above factors into account, homogeneous nucleation and stable

https://dx.doi.org/10.1021/acsami.0c05661
ACS Appl. Mater. Interfaces 2020, 12, 23028−23034

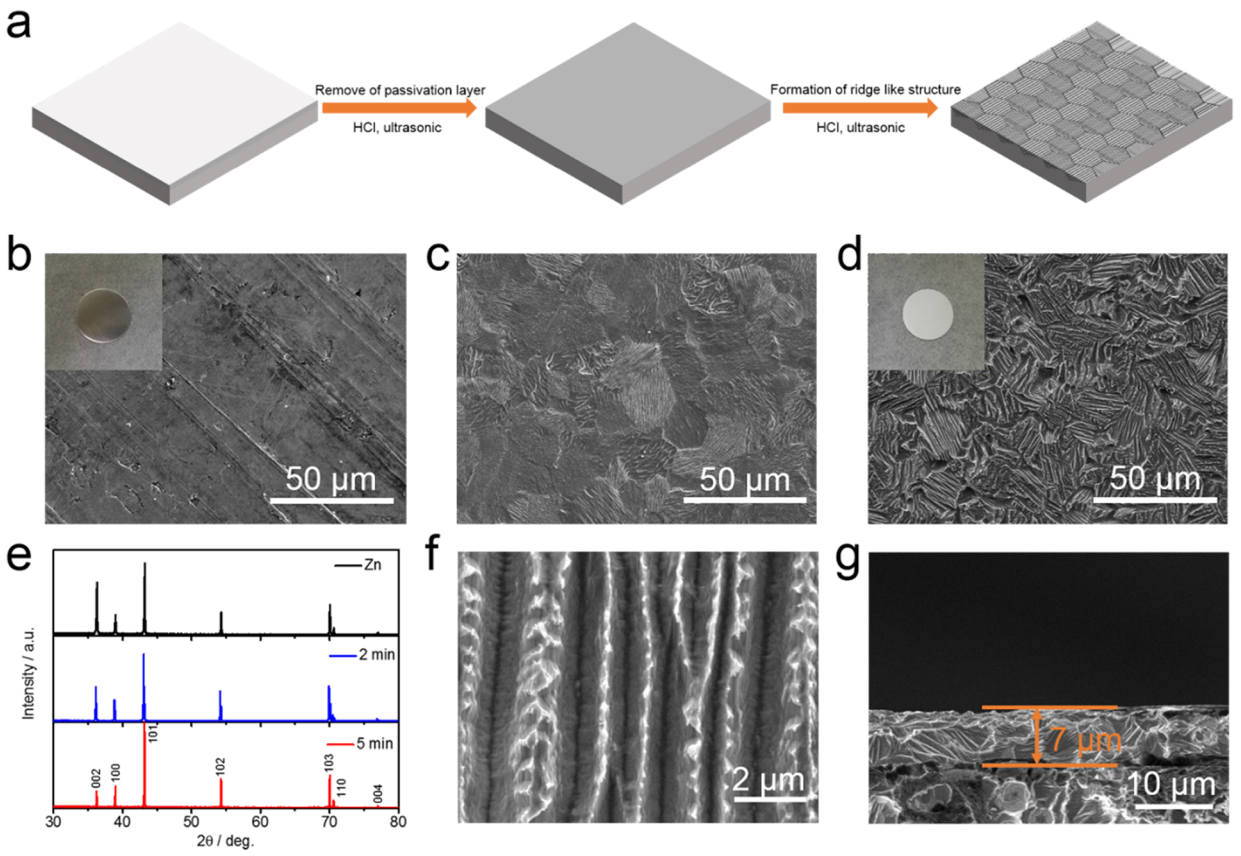

Figure 2. (a) Schematic illustration of the fabrication process of the r-Zn foil anode. Top-view SEM images of (b) pristine Zn foil, (c) Zn foil after etching for 2 min, and (d) Zn foil after etching for 5 min. The insets in (b) and (d) are digital images for the corresponding electrodes. (e) XRD patterns of pristine Zn and Zn foils after etching for 2 and 5 min. (f) High-resolution top-view SEM image of the r-Zn foil. (g) Cross-sectional SEM image of the r-Zn foil.

electrochemical plating/stripping behavior of metallic Zn can be expected for the as-designed r-Zn electrode.

An ultrasonic-assisted chemical etching method was employed to remove the native passivation layer of Zn foil, as illustrated in Figure 2a. SEM was first carried out to track the morphology evolution during the chemical etching. The surface of pristine Zn foil was relatively smooth except for some streaks, which were probably produced during its fabrication (Figure 2b). After chemical etching for 2 min, the initial smooth surface became rough, and aligned crystallographic planes of metallic Zn were observed in local areas with a size of ∼30 μm (Figure 2c), implying that the initial passivation layer on the very surface of the pristine Zn foil was removed, and a certain crystallographic orientation of hexagonal metallic Zn was exposed. This change in the surface structure of the Zn foil was also identified by the naked eye. The initial silver white for the pristine Zn foil turned pale white for the r-Zn foil (inset of Figure 2b, 2d). After chemical etching for 5 min, the crystallographic planes of metallic Zn were further developed, and the 3D ridge-like structure was formed on the surface of the Zn foil (Figure 2d), suggesting the preferential etching to produce certain exposed crystallographic planes of hexagonal metallic Zn. XRD was performed to investigate the ridge-like structure of the metallic Zn electrode and its formation mechanism. As shown in Figure 2e, the XRD peaks for pristine Zn foil matched well with the standard hexagonal-phased metallic Zn (JCPDS No. 04-0831). With the increase of etching time (e.g., 2 and 5 min), the relative intensity for the (002) peak of metallic Zn decreased (e.g., $I_{(002)}$:$I_{(100)}$:$I_{(101)}$ = 0.74:0.30:1 at 0 min, $I_{(002)}$:$I_{(100)}$:$I_{(101)}$ = 0.51:0.32:1 at 2 min, and $I_{(002)}$:$I_{(100)}$:$I_{(101)}$ = 0.20:0.27:1 at 5 min). The as-received commercial Zn foil was polycrystalline covered with a native passivation layer on the surface. This passivation layer could be removed in the initial stage of the chemical etching process, leaving a clean surface with a large number of grain boundaries and defects exposed. Such a surface structure was more active than the bulk structure of metallic Zn and therefore etched preferentially in the subsequent etching process. As is known, the (002) crystal plane is densely arranged and relatively more stable than other planes in the hexagonal-phased Zn metal.[42,43] The fast etching of other crystal planes led to the decrease in the proportion of the exposed (002) plane, which was consistent with the XRD results (Figure 2e). Taken together, the formation of the 3D ridge-like morphology is attributed to the selective etching of grain boundaries and crystallographic planes of metallic Zn, as demonstrated by the SEM and XRD results (Figure 2b–e). Further prolonging the etching time to 15 min led to the collapse of the foil structure (Figure S1). Therefore, the etching time was fixed as 5 min in the subsequent studies. The 3D ridge-like structure for the r-Zn anode was further studied by SEM (Figure 2f,g). The average width and depth of the ridges were ∼1 and ∼7 μm, respectively. Moreover, the surface of the ridge structure for the r-Zn foil was relatively rough in comparison to the pristine Zn foil (Figure S2). The electrochemical double-layer capacitance (C_{dl}) can reflect the electrochemical surface active area of an electrode. As shown in Table S1, the C_{dl} of the r-Zn electrode was determined to be

https://dx.doi.org/10.1021/acsami.0c05661
ACS Appl. Mater. Interfaces 2020, 12, 23028−23034

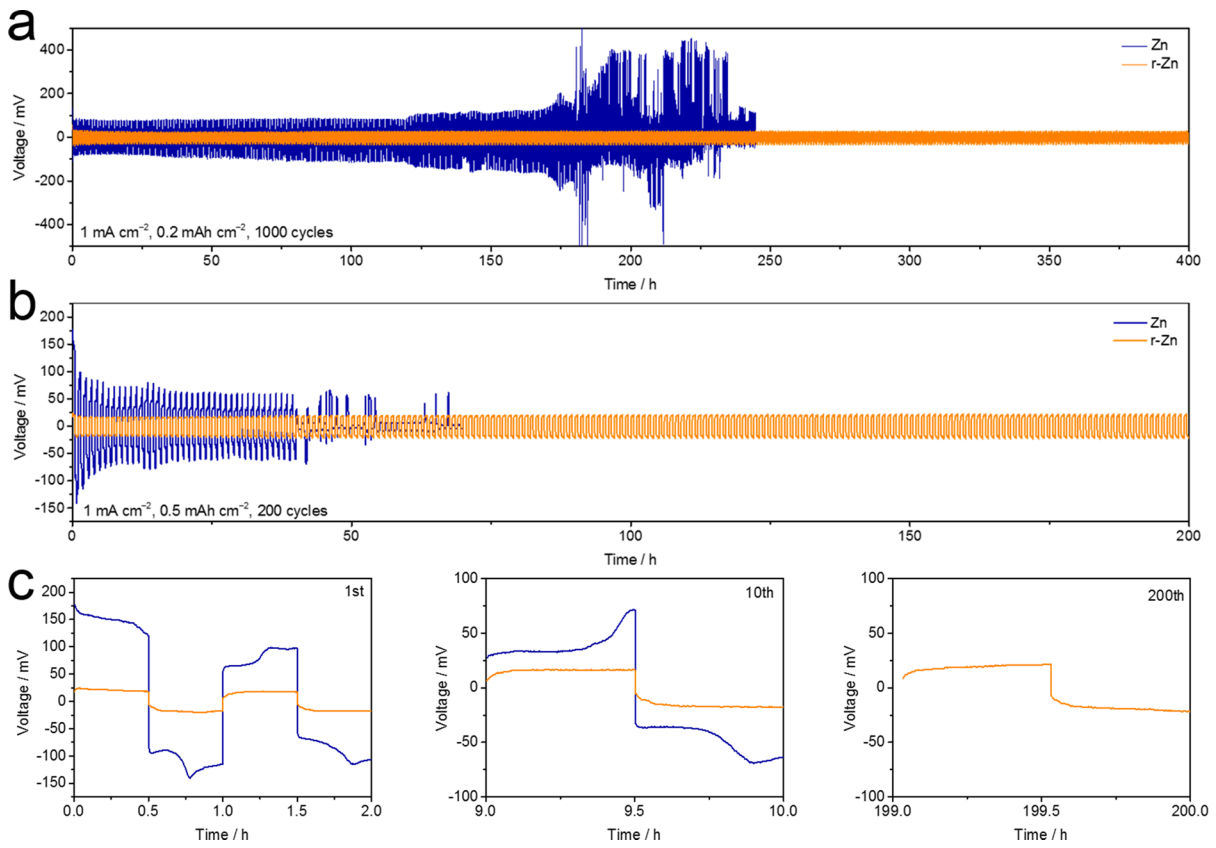

Figure 3. Voltage profiles of Zn || Zn and r-Zn || r-Zn symmetric cells at (a) 1 mA cm^{-2} and 0.2 mA h cm^{-2} and (b) 1 mA cm^{-2} and 0.5 mA h cm^{-2}. (c) The high-resolution voltage profiles for the 1st, 10th, and 200th cycles for the Zn || Zn and r-Zn || r-Zn symmetric cells at 1 mA cm^{-2} and 0.5 mA h cm^{-2}.

9.67 μF cm^{-2}, which was 12 times that of pristine Zn (0.79 μF cm^{-2}), demonstrating the significantly increased electrochemical surface area for the r-Zn electrode. The clean surface of the r-Zn electrode is beneficial for the uniform electrochemical deposition of metallic Zn. The continuous ridge structure and its rough surface can increase the accessible surface area to the electrolyte, thus reducing the risk for dendrite formation and improving the rate capability of the r-Zn electrode.

To investigate the electrochemical property of the r-Zn electrode, r-Zn || r-Zn symmetric cells were assembled using the aqueous $ZnSO_4$ electrolyte. As shown in Figure 3a, the r-Zn electrode exhibited stable electrochemical plating/stripping behavior with an overpotential of 26 mV for 400 h (1000 cycles) at a current density of 1 mA cm^{-2} and an areal capacity of 0.2 mA h cm^{-2}. In contrast, the pristine Zn electrode showed a much shorter lifespan of 180 h (450 cycles) with a much higher overpotential of 77 mV under the same condition. These results demonstrated the enhanced electrochemical performance of the r-Zn electrode with a fresh surface and 3D ridge-like structure. To further examine the practicability of the r-Zn electrode, the fixed areal capacity for testing was increased to 0.5 mA h cm^{-2}. The r-Zn || r-Zn symmetrical cells maintained stable electrochemical plating/stripping cycling for 200 h (200 cycles) at 1 mA cm^{-2} and 0.5 mA h cm^{-2}. In sharp contrast, the Zn || Zn symmetrical cells failed after 39 h (39 cycles) under the same test condition, which further demonstrated the important role of the clean surface and 3D ridge-like structure in improving the electrochemical cycling stability of the Zn electrode. In addition to the cycling stability, the r-Zn electrode showed an overpotential of 24 mV in the first cycle, which was only 1/7 of that of pristine Zn (177 mV, Figure 3c). Such improvement could be attributed to the removal of the surface passivation layer and the enlarged electrochemically active area for the r-Zn electrode. After 10 cycles, the overpotential of the pristine Zn electrode decreased to 72 mV, and the electrode was activated. The passivation layer on the pristine Zn electrode was detrimental to the electrochemical plating/stripping behavior, which reduced electrical conductivity and limited the diffusion of Zn ions. For the r-Zn electrode, the overpotential was ~20 mV at the 10th cycle, which was nearly the same as that at the 1st cycle, suggesting the improved kinetics of the plating/stripping behavior of metallic Zn after our chemical etching procedure. The r-Zn electrode also shows advancement in overpotential in comparison to many of the recently reported Zn metal electrodes (Table S2). The r-Zn electrode displayed stable cycling for over 200 cycles and exhibited a low overpotential of 22 mV for the 200th cycle, which was much lower than that for pristine Zn after activation (72 mV, 10th cycle). The low overpotential of the r-Zn electrodes reflected the fast ion transport at the electrode/electrolyte interface,[15,44,45] which could also be attributed to the clean surface and 3D ridge-like structure on the as-designed r-Zn electrode. Besides, the r-Zn electrode showed stable Zn plating/stripping behavior for 56 h (280 cycles) at 5 mA cm^{-2} and 0.5 mA h cm^{-2} (Figure S3). In contrast, the pristine Zn electrode showed a much shorter lifespan of 27 h (135 cycles) under the same test condition, demonstrating the improved electrochemical performance of the r-Zn electrode.

https://dx.doi.org/10.1021/acsami.0c05661
ACS Appl. Mater. Interfaces 2020, 12, 23028−23034

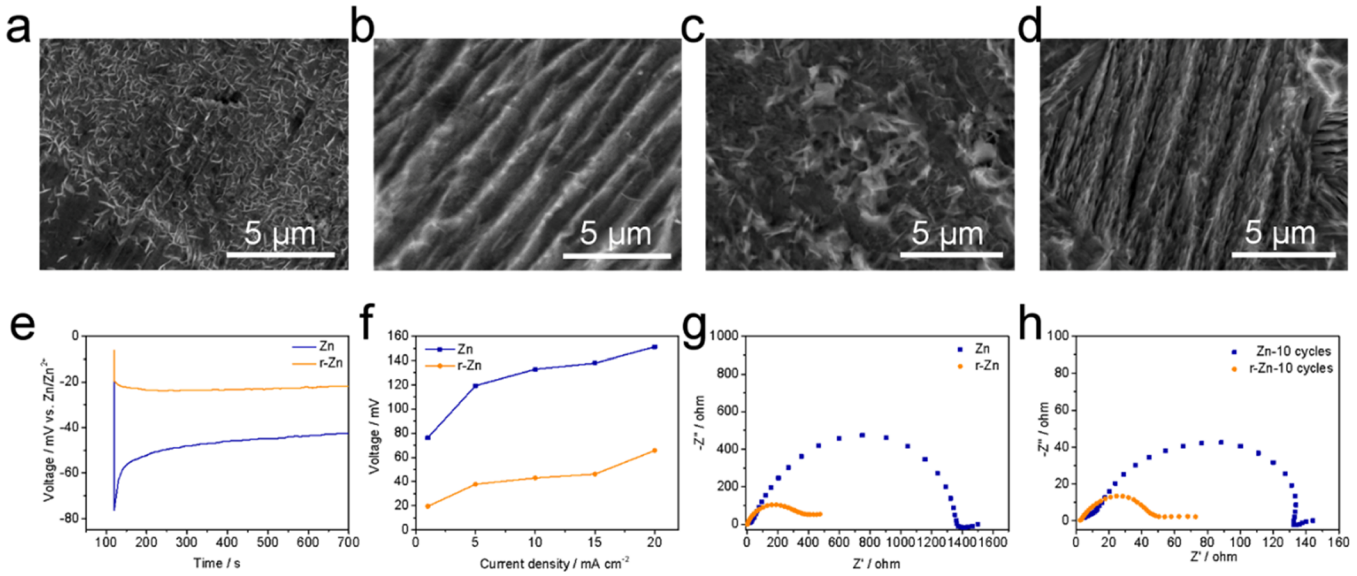

Figure 4. SEM images of the surface of (a) pristine Zn and (b) r-Zn foil electrodes after electrochemical plating of 0.5 mA h cm^{-2} of metallic Zn. SEM images of the surface of (c) pristine Zn and (d) r-Zn foil electrodes after 10 plating/stripping cycles at 1 mA cm^{-2} and 0.5 mA h cm^{-2}. (e) The voltage−time curves for pristine Zn and r-Zn anode during Zn nucleation at 1 mA cm^{-2}. (f) The nucleation overpotential of pristine Zn and r-Zn foil electrodes at different current densities. Nyquist plots of pristine Zn and r-Zn foil electrodes (g) before cycling and (h) after 10 plating/stripping cycles at 1 mA cm^{-2} and 0.5 mA h cm^{-2}.

The r-Zn electrode with clean surface and high electrochemical activity can avoid the nonuniform deposition of metallic Zn during the plating/stripping cycling. As shown in Figure 4a, nonuniform deposition behavior of metallic Zn was for the pristine Zn electrode at 0.5 mA h cm^{-2} and 1 mA cm^{-2}. We noted that the Zn metal was not uniformly plated on the pristine Zn electrode (Figure S4a). The native passivation layer of the pristine Zn electrode may lead to the uneven electric field during electrochemical plating due to its inhomogeneity in thickness and composition. In contrast, the r-Zn electrode maintained its initial morphology under the same condition after electrochemical plating (Figure 4b, Figure S4b), suggesting the uniform plating behavior of the r-Zn electrode. To verify the stability of the 3D ridge-like structure, 0.5 mA h cm^{-2} of metallic Zn was stripped from the r-Zn electrode at 1 mA cm^{-2}. The initial structure of the r-Zn electrode was well maintained, indicating its uniform stripping behavior. In contrast, a number of pits were observed on the surface of the pristine Zn electrode after the same stripping process (Figure S5), suggesting the much improved electrochemical stripping behavior of metallic Zn after the removal of the native surface passivation layer. Moreover, after 10 plating/stripping cycles at 1 mA cm^{-2} and 0.5 mA h cm^{-2}, a large number of flaky Zn were formed on the pristine Zn electrode (Figure 4c, Figure S6a), which were stacked randomly. The random distribution of these as-formed Zn flakes would further cause the inhomogeneity of plating/stripping and produce "dead Zn", resulting in battery failure or loss in active Zn. For the r-Zn electrode, the overall morphology and structure were maintained well after 10 plating/stripping cycles (Figure 4d, Figure S6b), demonstrating the important role of a clean surface and 3D ridge-like structure in improving the cycling stability of the Zn metal electrode. The nonuniform plating of metallic Zn can be understood by the nucleation overpotential during electrochemical plating.[15,46] Smaller nucleation overpotential demonstrated smaller nucleation resistance and easier nucleation behavior, and thus, a large number of nucleus of crystallization were produced, leading to uniform deposition of metallic Zn. As shown in Figure 4e, the pristine Zn electrode underwent a sharp voltage drop to 75 mV at 1 mA cm^{-2}. In contrast, the r-Zn electrode showed almost no voltage drop, and the voltage response was stable during the whole plating process, indicating the uniform nucleation and plating process. At various current densities, the r-Zn electrode maintained a lower nucleation overpotential than the pristine Zn electrode (Figure 4f). Even at the current density as high as 20 mA cm^{-2}, the overpotential of the r-Zn electrode was only 60 mV, much lower than the value in the previous work.[15] Also, stable voltage was observed during the entire plating process (Figure S7). The above results suggested that the Zn plating/stripping process was more uniform for the r-Zn electrode than the pristine Zn electrode. Electrochemical impedance spectroscopy (EIS) was carried out to study the charge transfer on pristine Zn and r-Zn electrodes. As shown in Figure 4g, the charge transfer resistance of the r-Zn electrode before cycling was ∼380 Ω, much smaller than that of the pristine Zn electrode (∼1370 Ω), which should be mainly attributed to the removal of the surface passivation layer and the increased accessible surface area to the electrolyte. In addition, the solution resistance (R_s) for the r-Zn electrode was much smaller than that of pristine Zn (0.90 vs 18.39 Ω, Figure S8 and Table S1), indicating the significantly improved electronic conductivity of r-Zn after the removal of the native surface passivation layer. After electrochemical activation (10 plating/stripping cycles), the charge transfer resistance of both electrodes decreased. The charge transfer resistance of the r-Zn electrode was ∼50 Ω, which was much smaller than that of the pristine Zn electrode (∼140 Ω), demonstrating the important role of the fresh electrode surface and the 3D ridge-like structure on enlarging the electrochemical specific surface area and accelerating the mass transfer for the r-Zn electrode. All these above results revealed the improved reaction kinetics and stability of the r-Zn electrode due to the removal of the surface

https://dx.doi.org/10.1021/acsami.0c05661
ACS Appl. Mater. Interfaces 2020, 12, 23028−23034

passivation layer and the construction of the 3D ridge-like structure.

4. CONCLUSIONS

In summary, we reported the preparation of the r-Zn electrode with a clean surface and 3D ridge-like structure as a high-performance Zn metal anode for aqueous rechargeable batteries. The r-Zn anode was fabricated through a facile chemical etching method, during which the native pristine passivation surface layer was removed, and the 3D ridge-like structure with an increased electrochemically active surface was formed on the Zn foil electrode. The as-achieved r-Zn electrode showed accelerated mass transfer processes and thus stable electrochemical plating/stripping behavior with low overpotential without the formation of the undesirable Zn dendrite. The overpotential of the r-Zn electrode remained at 22 mV at 1 mA cm^{-2} and 0.5 mA h cm^{-2} after 200 h of cycling, much better than the pristine Zn electrode with a native passivation layer (e.g., 72 mV after 39 h of cycling). This work reveals the significant role of a clean surface on the electrochemical plating/stripping behavior of Zn metal electrodes, including the reduced overpotential, enhanced cycling stability, and suppression of dendrite growth, and also inspires the rational design and fabrication of the Zn metal electrode toward practical application for aqueous rechargeable batteries.

■ ASSOCIATED CONTENT

Supporting Information

The Supporting Information is available free of charge at https://pubs.acs.org/doi/10.1021/acsami.0c05661.

Digital image of the Zn foil after etching for 15 min, SEM images of pristine Zn foil, SEM images of pristine Zn foil or r-Zn foil after plating metallic Zn, stripping metallic Zn, and 10 plating/stripping cycles, and voltage−time curves during Zn nucleation on pristine Zn and r-Zn foil electrodes (PDF)

■ AUTHOR INFORMATION

Corresponding Author

Yongming Sun − *Wuhan National Laboratory for Optoelectronics and School of Optical and Electronic Information, Huazhong University of Science and Technology, Wuhan 430074, China;* orcid.org/0000-0001-8528-525X; Email: yongmingsun@hust.edu.cn

Authors

Jindi Wang − *Wuhan National Laboratory for Optoelectronics and School of Optical and Electronic Information, Huazhong University of Science and Technology, Wuhan 430074, China*

Zhao Cai − *Wuhan National Laboratory for Optoelectronics and School of Optical and Electronic Information, Huazhong University of Science and Technology, Wuhan 430074, China;* orcid.org/0000-0001-7110-9300

Run Xiao − *Wuhan National Laboratory for Optoelectronics and School of Optical and Electronic Information, Huazhong University of Science and Technology, Wuhan 430074, China*

Yangtao Ou − *Wuhan National Laboratory for Optoelectronics and School of Optical and Electronic Information, Huazhong University of Science and Technology, Wuhan 430074, China*

Renming Zhan − *Wuhan National Laboratory for Optoelectronics and School of Optical and Electronic Information, Huazhong University of Science and Technology, Wuhan 430074, China*

Zhu Yuan − *Wuhan National Laboratory for Optoelectronics and School of Optical and Electronic Information, Huazhong University of Science and Technology, Wuhan 430074, China*

Complete contact information is available at: https://pubs.acs.org/10.1021/acsami.0c05661

Author Contributions

‡J.W. and Z.C. contributed equally.

Notes

The authors declare no competing financial interest.

■ ACKNOWLEDGMENTS

Y.S. acknowledges the financial support by the Innovation Fund of Wuhan National Laboratory for Optoelectronics of Huazhong University of Science and Technology. Z.C. thanks the China Postdoctoral Science Foundation (No. 2018M640694). The authors would like to thank the Analytical and Testing Center of Huazhong University of Science and Technology as well as the Center for Nanoscale Characterization & Devices of Wuhan National Laboratory for Optoelectronics for providing the facilities to conduct the characterization.

■ REFERENCES

(1) Dunn, B.; Kamath, H.; Tarascon, J.-M. Electrical Energy Storage for the Grid: A Battery of Choices. *Science* **2011**, *334*, 928−935.

(2) Chu, S.; Majumdar, A. Opportunities and Challenges for a Sustainable Energy Future. *Nature* **2012**, *488*, 294−303.

(3) Chu, S.; Cui, Y.; Liu, N. The Path towards Sustainable Energy. *Nat. Mater.* **2016**, *16*, 16−22.

(4) Fang, G.; Zhou, J.; Pan, A.; Liang, S. Recent Advances in Aqueous Zinc-Ion Batteries. *ACS Energy Lett.* **2018**, *3*, 2480−2501.

(5) Song, M.; Tan, H.; Chao, D.; Fan, H. J. Recent Advances in Zn-Ion Batteries. *Adv. Funct. Mater.* **2018**, *28*, 1802564.

(6) Zeng, X.; Hao, J.; Wang, Z.; Mao, J.; Guo, Z. Recent Progress and Perspectives on Aqueous Zn-Based Rechargeable Batteries with Mild Aqueous Electrolytes. *Energy Storage Mater.* **2019**, *20*, 410−437.

(7) Li, H.; Ma, L.; Han, C.; Wang, Z.; Liu, Z.; Tang, Z.; Zhi, C. Advanced Rechargeable Zinc-Based Batteries: Recent Progress and Future Perspectives. *Nano Energy* **2019**, *62*, 550−587.

(8) Konarov, A.; Voronina, N.; Jo, J. H.; Bakenov, Z.; Sun, Y.-K.; Myung, S.-T. Present and Future Perspective on Electrode Materials for Rechargeable Zinc-Ion Batteries. *ACS Energy Lett.* **2018**, *3*, 2620−2640.

(9) Chen, L.; Yang, Z.; Huang, Y. Monoclinic VO_2 Hollow Nanospheres with Super-Long Cycle Life for Aqueous Zinc Ion Batteries. *Nanoscale* **2019**, *11*, 13032−13039.

(10) Kundu, D.; Vajargah, S. H.; Wan, L.; Adams, B.; Prendergast, D.; Nazar, L. F. Aqueous vs. nonaqueous Zn-ion batteries: consequences of the desolvation penalty at the interface. *Energy Environ. Sci.* **2018**, *11*, 881−892.

(11) Huang, J.; Guo, Z.; Ma, Y.; Bin, D.; Wang, Y.; Xia, Y. Recent Progress of Rechargeable Batteries Using Mild Aqueous Electrolytes. *Small Methods* **2019**, *3*, 1800272.

(12) Liu, T.; Cheng, X.; Yu, H.; Zhu, H.; Peng, N.; Zheng, R.; Zhang, J.; Shui, M.; Cui, Y.; Shu, J. An Overview and Future Perspectives of Aqueous Rechargeable Polyvalent Ion Batteries. *Energy Storage Mater.* **2019**, *18*, 68−91.

(13) Li, Y.; Fu, J.; Zhong, C.; Wu, T.; Chen, Z.; Hu, W.; Amine, K.; Lu, J. Recent Advances in Flexible Zinc-Based Rechargeable Batteries. *Adv. Energy Mater.* **2019**, *9*, 1802605.

(14) Yi, J.; Liang, P.; Liu, X.; Wu, K.; Liu, Y.; Wang, Y.; Xia, Y.; Zhang, J. Challenges, Mitigation Strategies and Perspectives in Development of Zinc-Electrode Materials and Fabrication for

Rechargeable Zinc−Air Batteries. *Energy Environ. Sci.* **2018**, *11*, 3075−3095.
(15) Zeng, Y.; Zhang, X.; Qin, R.; Liu, X.; Fang, P.; Zheng, D.; Tong, Y.; Lu, X. Dendrite-Free Zinc Deposition Induced by Multifunctional CNT Frameworks for Stable Flexible Zn-Ion Batteries. *Adv. Mater.* **2019**, *31*, 1903675.
(16) Wang, F.; Borodin, O.; Gao, T.; Fan, X.; Sun, W.; Han, F.; Faraone, A.; Dura, J. A.; Xu, K.; Wang, C. Highly Reversible Zinc Metal Anode for Aqueous Batteries. *Nat. Mater.* **2018**, *17*, 543−549.
(17) Lu, W.; Xie, C.; Zhang, H.; Li, X. Inhibition of Zinc Dendrite Growth in Zinc-Based Batteries. *ChemSusChem* **2018**, *11*, 3996−4006.
(18) Yang, Q.; Liang, G.; Guo, Y.; Liu, Z.; Yan, B.; Wang, D.; Huang, Z.; Li, X.; Fan, J.; Zhi, C. Do Zinc Dendrites Exist in Neutral Zinc Batteries: A Developed Electrohealing Strategy to In Situ Rescue In-Service Batteries. *Adv. Mater.* **2019**, *31*, 1903778.
(19) Zhou, F.; Lin, Y.; Li, T.; Zhang, S.; Deng, C. Forming Bubble-Encapsulated Double-Shelled Hollow Spheres towards Fast Kinetics and Superior High Rate Performance for Aqueous Rechargeable Zn-Ion Batteries. *J. Mater. Chem. A* **2019**, *7*, 10589−10600.
(20) Dai, X.; Wan, F.; Zhang, L.; Cao, H.; Niu, Z. Freestanding Graphene/VO_2 Composite Films for Highly Stable Aqueous Zn-Ion Batteries with Superior Rate Performance. *Energy Storage Mater.* **2019**, *17*, 143−150.
(21) Jiang, L.; Wu, Z.; Wang, Y.; Tian, W.; Yi, Z.; Cai, C.; Jiang, Y.; Hu, L. Ultrafast Zinc-Ion Diffusion Ability Observed in 6.0-Nanometer Spinel Nanodots. *ACS Nano* **2019**, *13*, 10376−10385.
(22) Kang, L.; Cui, M.; Jiang, F.; Gao, Y.; Luo, H.; Liu, J.; Liang, W.; Zhi, C. Nanoporous $CaCO_3$ Coatings Enabled Uniform Zn Stripping/Plating for Long-Life Zinc Rechargeable Aqueous Batteries. *Adv. Energy Mater.* **2018**, *8*, 1801090.
(23) Zhao, Z.; Zhao, J.; Hu, Z.; Li, J.; Li, J.; Zhang, Y.; Wang, C.; Cui, G. Long-life and Deeply Rechargeable Aqueous Zn Anodes Enabled by a Multifunctional Brightener-Inspired Interphase. *Energy Environ. Sci.* **2019**, *12*, 1938−1949.
(24) Wang, Z.; Hu, J.; Han, L.; Wang, Z.; Wang, H.; Zhao, Q.; Liu, J.; Pan, F. A MOF-Based Single-Ion Zn^{2+} Solid Electrolyte Leading to Dendrite-Free Rechargeable Zn Batteries. *Nano Energy* **2019**, *56*, 92−99.
(25) Zeng, Y.; Zhang, X.; Meng, Y.; Yu, M.; Yi, J.; Wu, Y.; Lu, X.; Tong, Y. Achieving Ultrahigh Energy Density and Long Durability in a Flexible Rechargeable Quasi-Solid-State Zn-MnO_2 Battery. *Adv. Mater.* **2017**, *29*, 1700274.
(26) Han, Q.; Chi, X.; Zhang, S.; Liu, Y.; Zhou, B.; Yang, J.; Liu, Y. Durable, Flexible Self-Standing Hydrogel Electrolytes Enabling High-Safety Rechargeable Solid-State Zinc Metal Batteries. *J. Mater. Chem. A* **2018**, *6*, 23046−23054.
(27) Li, H.; Han, C.; Huang, Y.; Huang, Y.; Zhu, M.; Pei, Z.; Xue, Q.; Wang, Z.; Liu, Z.; Tang, Z.; Wang, Y.; Kang, F.; Li, B.; Zhi, C. An Extremely Safe and Wearable Solid-State Zinc Ion Battery Based on a Hierarchical Structured Polymer Electrolyte. *Energy Environ. Sci.* **2018**, *11*, 941−951.
(28) Wang, Z.; Ruan, Z.; Liu, Z.; Wang, Y.; Tang, Z.; Li, H.; Zhu, M.; Hung, T. F.; Liu, J.; Shi, Z.; Zhi, C. A Flexible Rechargeable Zinc-Ion Wire-Shaped Battery with Shape Memory Function. *J. Mater. Chem. A* **2018**, *6*, 8549−8557.
(29) Cao, H.; Wan, F.; Zhang, L.; Dai, X.; Huang, S.; Liu, L.; Niu, Z. Highly Compressible Zinc-Ion Batteries with Stable Performance. *J. Mater. Chem. A* **2019**, *7*, 11734−11741.
(30) Wan, F.; Zhang, L.; Dai, X.; Wang, X.; Niu, Z.; Chen, J. Aqueous Rechargeable Zinc/Sodium Vanadate Batteries with Enhanced Performance from Simultaneous Insertion of Dual Carriers. *Nat. Commun.* **2018**, *9*, 1656.
(31) Chamoun, M.; Brant, W. R.; Tai, C.-W.; Karlsson, G.; Noréus, D. Rechargeability of Aqueous Sulfate Zn/MnO_2 Batteries Enhanced by Accessible Mn^{2+} Ions. *Energy Storage Mater.* **2018**, *15*, 351−360.
(32) Pan, H.; Shao, Y.; Yan, P.; Cheng, Y.; Han, K. S.; Nie, Z.; Wang, C.; Yang, J.; Li, X.; Bhattacharya, P.; Mueller, K. T.; Liu, J. Reversible Aqueous Zinc/Manganese Oxide Energy Storage from Conversion Reactions. *Nat. Energy* **2016**, *1*, 16039.
(33) Parker, J. F.; Chervin, C. N.; Pala, I. R.; Machler, M.; Burz, M. F.; Long, J. W.; Rolison, D. R. Rechargeable Nickel-3D Zinc Batteries: An Energy-Dense, Safer Alternative to Lithium-Ion. *Science* **2017**, *356*, 415−418.
(34) Dong, W.; Shi, J.-L.; Wang, T.-S.; Yin, Y.-X.; Wang, C.-R.; Guo, Y.-G. Zinc@Carbon Fiber Composite Framework Anode for Aqueous Zn-MnO_2 Batteries. *RSC Adv* **2018**, *8*, 19157−19163.
(35) Chao, D.; Zhu, C. R.; Song, M.; Liang, P.; Zhang, X.; Tiep, N. H.; Zhao, H.; Wang, J.; Wang, R.; Zhang, H.; Fan, H. J. A High-Rate and Stable Quasi-Solid-State Zinc-Ion Battery with Novel 2D Layered Zinc Orthovanadate Array. *Adv. Mater.* **2018**, *30*, 1803181.
(36) Li, H.; Liu, Z.; Liang, G.; Huang, Y.; Huang, Y.; Zhu, M.; Pei, Z.; Xue, Q.; Tang, Z.; Wang, Y.; Li, B.; Zhi, C. Waterproof and Tailorable Elastic Rechargeable Yarn Zinc Ion Batteries by a Cross-Linked Polyacrylamide Electrolyte. *ACS Nano* **2018**, *12*, 3140−3148.
(37) Wang, Z.; Huang, J.; Guo, Z.; Dong, X.; Liu, Y.; Wang, Y.; Xia, Y. A Metal-Organic Framework Host for Highly Reversible Dendrite-Free Zinc Metal Anodes. *Joule* **2019**, *3*, 1289−1300.
(38) Zhao, J.; Ren, H.; Liang, Q.; Yuan, D.; Xi, S.; Wu, C.; Manalastas, W., Jr.; Ma, J.; Fang, W.; Zheng, Y.; Du, C.-F.; Srinivasan, M.; Yan, Q. High-Performance Flexible Quasi-Solid-State Zinc-Ion Batteries with Layer-Expanded Vanadium Oxide Cathode and Zinc/Stainless Steel Mesh Composite Anode. *Nano Energy* **2019**, *62*, 94−102.
(39) Li, M.; He, Q.; Li, Z.; Li, Q.; Zhang, Y.; Meng, J.; Liu, X.; Li, S.; Wu, B.; Chen, L.; Liu, Z.; Luo, W.; Han, C.; Mai, L. A Novel Dendrite-Free Mn^{2+}/Zn^{2+} Hybrid Battery with 2.3 V Voltage Window and 11000-Cycle Lifespan. *Adv. Energy Mater.* **2019**, *9*, 1901469.
(40) Graedel, T. Corrosion Mechanisms for Zinc Exposed to the Atmosphere. *J. Electrochem. Soc.* **1989**, *136*, 193C−203C.
(41) Friel, J. J. Atmospheric Corrosion Products on Al, Zn, and AlZn Metallic Coatings. *Corrosion* **1986**, *42*, 422−426.
(42) Qian, B.; Shen, Z. Fabrication of Superhydrophobic Surfaces by Dislocation-Selective Chemical Etching on Aluminum, Copper, and Zinc Substrates. *Langmuir* **2005**, *21*, 9007−9009.
(43) Wang, H.; Yang, Z.; Yu, J.; Wu, Y.; Shao, W.; Jiang, T.; Xu, X. Preparation of Lotus-Like Hierarchical Microstructures on Zinc Substrate and Study of Its Wettability. *RSC Adv.* **2014**, *4*, 33730−33738.
(44) Jiao, T.; Yang, Q.; Wu, S.; Wang, Z.; Chen, D.; Shen, D.; Liu, B.; Cheng, J.; Li, H.; Ma, L.; Zhi, C.; Zhang, W. Binder-Free Hierarchical VS_2 Electrodes for High-Performance Aqueous Zn Ion Batteries towards Commercial Level Mass Loading. *J. Mater. Chem. A* **2019**, *7*, 16330−16338.
(45) Zhang, N.; Cheng, F.; Liu, Y.; Zhao, Q.; Lei, K.; Chen, C.; Liu, X.; Chen, J. Cation-Deficient Spinel $ZnMn_2O_4$ Cathode in Zn-$(CF_3SO_3)_2$ Electrolyte for Rechargeable Aqueous Zn-Ion Battery. *J. Am. Chem. Soc.* **2016**, *138*, 12894−12901.
(46) Kim, Y.-J.; Kwon, S. H.; Noh, H.; Yuk, S.; Lee, H.; Jin, H. S.; Lee, J.; Zhang, J.-G.; Lee, S. G.; Guim, H.; Kim, H.-T. Facet Selectivity of Cu Current Collector for Li Electrodeposition. *Energy Storage Mater.* **2019**, *19*, 154−162.

https://dx.doi.org/10.1021/acsami.0c05661
ACS Appl. Mater. Interfaces 2020, 12, 23028−23034